Cent. Eur. J. Phys. • 10(1) • 2012 • 172-180
DOI: 10.2478/s11534-011-0095-3

VERSITA

Central European Journal of **Physics**

Energy-loss function of TTF-TCNQ

Research Article

Željana Bonačić Lošić[1]*

1 *University of Split, Faculty of Science, Teslina 12, 21000 Split, Croatia*

Received 23 May 2011; accepted 13 October 2011

Abstract: We investigate the energy-loss function for a previously developed model of quasi-one-dimensional metals with two one-dimensional electron bands per donor and acceptor chains and the three-dimensional long-range Coulomb electron-electron interaction within the random phase approximation. It is essentially influenced by two hybridized collective modes which result from the strong coupling of the intraband plasmon and the interband dipolar modes. Our calculations show that the spectral weights of the renormalized plasmon and the dipolar mode dominate within the long wavelength limit, while for large longitudinal wave vectors the intraband electron-hole quasi-continuum gains some experimentally observable spectral weight as the second mode approaches it. The function obtained is brought into correspondence with the data of the quasi-one-dimensional organic conductor tetrathiafulvalene-tetracyanoquinodimethane (TTF-TCNQ) obtained from electron energy-loss spectroscopy (EELS) measurements.

PACS (2008): 71.45.Gm,77.84.Jd,78.30.Jw

Keywords: dielectric response • collective modes • loss-function

© *Versita Sp. z o.o.*

1. Introduction

The most intensely studied quasi-one-dimensional organic conductor, tetrathiafulvalene-tetracyanoquinodimethane (TTF-TCNQ), holds promise for potential use in organic electronics due to possible advances in application as a contact electrode as well as an active layer of organic field-effect transistors (OFETs) [1–4]. However, efficient models for the screened Coulomb interaction are necessary for the further development of the exploitation of new device applications and the microscopic understanding of optical and electronic properties. The Coulomb electron-electron interaction and its dynamical screening due to many-body effects is an important property of the organic conductor TTF-TCNQ. Dynamical screening determines its spectral properties and collective modes. Experimentally, the collective modes can be investigated by electron energy-loss spectroscopy (EELS) [5–7] and essentially influence the spectrum obtained by angle-resolved photoemission spectroscopy (ARPES) [8–11]. In this paper we are focused on understanding the energy-loss function of TTF-TCNQ.

Early measurements of the energy loss of TTF-TCNQ [12] have shown a strong angular dependence of excitation at 0.75 eV which was in qualitative agreement with the dispersion of the plasmon mode in the model of a quasi-one-

*E-mail: agicz@pmfst.hr

dimensional conductor with one one-dimensional electron band per chain based on the random phase approximation (RPA) proposed by Williams and Bloch [13] and the extended models proposed by Williams and Bloch [14] and Kahn et al. [15]. The width of this excitation increases as the momentum increases. The extended models comprised two one-dimensional electron bands, each on a different type of chain, and they have predicted a second excitation. Williams and Bloch have found that the second coupled plasmon mode is acoustic, but it is still placed above the electron-hole quasi-continuum, whereas Kahn et al. have shown the existence of the acoustic collective mode in the narrow region between the quasi-continuums of two sublattices where its weak strength makes it experimentally unobservable. Furthermore, in the wide temperature range up to above room temperature (i. e. far above the range of charge density wave instabilities that occur below 60K in TTF-TCNQ) far-infrared optical measurements have revealed an unusual low-frequency optical mode at approximately 10 meV [16–18]. The models of [14, 15] do not apply to TTF-TCNQ which has four conducting bands (two per each type of chains) and the observed combination of collective modes originates from their presence [19].

Previously, in Ref. [20] Bonačić Lošić and Županović investigated the collective excitation spectrum for the model of a quasi-one-dimensional conductor, proposed in Ref. [19] within RPA, with two one-dimensional electron bands per donor and acceptor chains, with the lower bands being partially filled and the upper empty, along with the three-dimensional long-ranged Coulomb electron-electron interaction. Due to these bands and the three dimensional Coulomb electron-electron interaction there is a strong hybridization between initial intraband plasmons and interband dipolar modes. Their calculations also showed the existence of the acoustic mode placed between the acceptor and donor quasi-continuums in the long wavelength limit. Additionally, there were three collective modes above both electron-hole quasi-continuums: two of them, the renormalised plasmon and dipolar mode, were brought into correspondence with the observed modes at 10 meV and 0.75 eV, respectively.

We mention that RPA has been extensively employed to analyse the linear response of the three-dimensional "jellium" model [5] and more recently that of layered electron systems such as double quantum wells [21], one-dimensional quantum wires [22], double quantum wires [23], graphene [24–27] and double layer graphene [28] which have the collective mode spectra that differ fundamentally from those of the three-dimensional electron systems as they contain low-energy collective modes due to their reduced dimensionality.

In this paper, our analysis extends our original work [20] in the approach of Ref. [19] in order to calculate the screened monopole-monopole Coulomb electron-electron interaction, the macroscopic dielectric function and the energy-loss function. The screened Coulomb interaction displays strong dynamical behavior originating from the collective modes obtained. The energy-loss function has a negligible contribution from electron-hole quasi-continuums and from the acoustic collective mode between them in the long wavelength limit, in agreement with the experiments which found them unobservable. The spectral weight is distributed between the collective modes above both electron-hole quasi-continuums. At intermediate wave vectors, the renormalised plasmon mode corresponding to the 10 meV mode blends with the electron-hole quasi-continuum and most of its spectral weight is transferred to the renormalised dipolar mode corresponding to the 0.75 eV mode. At large wave vectors, the spectral weight of the renormalised dipolar mode dominates, and the electron-hole quasi-continuum gains some spectral weight as the former slightly approaches the latter. This is in qualitative agreement with the experimental observation that the width of the excitation at 0.75 eV increases as the momentum increases along with its negative dispersion [12].

The work presented here is in zero temperature formalism and it is consistent with the experimental results in the broad temperature range from 60 K up to 300 K [12, 16–18]. It would also be interesting to see if the observed features could be reproduced by finite temperature calculations. The full discussion on the extension to the case of $T \neq 0$ will be given elsewhere[1]. In this respect here we only recall how the formalism should be modified to handle effectively non zero conditions.

In Section 2, we describe the model we used and we present a discussion of our results for the screened monopole-monopole Coulomb matrix element. In Section 3, we evaluate the real and imaginary parts of the macroscopic dielectric function. In Section 4, we study the energy-loss function and show that it is in qualitative agreement with the EELS spectra of TTF-TCNQ. Our results are summarized and discussed in Section 5.

2. Screened interaction

The tight-binding formulation of the dielectric response for multi-band electron systems [19] starts with a linear

[1] *Ž. Bonačić Lošić, to be published*

system of RPA Dyson equations in $(\mathbf{q},\omega)$-space for the screened Coulomb electron-electron interaction

$$\sum_{p_g}[\delta_{p_e p_g} - V_{p_e p_g}(\mathbf{q})\Pi_{p_g}(\mathbf{q},\omega)]\bar{V}_{p_g p_f}(\mathbf{q},\omega) = V_{p_e p_f}(\mathbf{q}). \quad (1)$$

In general, electron-electron Coulomb interactions involve dynamical screening, included here by taking into account the effect of frequency-dependent polarization. Here $\Pi_{p_g}(\mathbf{q},\omega)$ are intraband and interband RPA polarization diagrams, and $V_{p_e p_f}(\mathbf{q})$ are matrix elements of the bare Coulomb electron-electron interaction between intraband or interband transitions, as indices $p_e = (l_e, l'_e)$ denote either interband ($l_e \neq l'_e$) or intraband ($l_e = l'_e$) transitions between orbitals l_e and l'_e. Also, e and f denote acceptor and donor molecules. The polarization diagrams are given by [29]

$$\Pi_{l_e l'_e}(\mathbf{q},\omega) = \frac{2}{N}\sum_{\mathbf{k}} \left\{ \frac{[1-n_{l_e}(\mathbf{k})]n_{l'_e}(\mathbf{k}+\mathbf{q})}{\omega + E_{l'_e}(\mathbf{k}+\mathbf{q}) - E_{l_e}(\mathbf{k}) + i\eta} - \frac{n_{l_e}(\mathbf{k})[1-n_{l'_e}(\mathbf{k}+\mathbf{q})]}{\omega + E_{l'_e}(\mathbf{k}+\mathbf{q}) - E_{l_e}(\mathbf{k}) - i\eta} \right\}, \quad (2)$$

where $n_{l_e}(\mathbf{k})$ is the Fermi-Dirac distribution and $E_{l_e}(\mathbf{k})$ is the single-particle energy dispersion curve. For $T \neq 0$ $n_{l_e}(\mathbf{k}) = \left\{1 + exp\left[\frac{E_{l_e}(\mathbf{k})-\mu}{k_B T}\right]\right\}^{-1}$, where k_B is the Boltzman constant and the chemical potential μ can be determined self-consistently from the conservation of total number of particles

$$N = 2\sum_{l_e \mathbf{k}} n_{l_e}(\mathbf{k}), \quad (3)$$

where the 2 comes from the spin degeneracy. The present work is concerned with the T=0 formalism which takes $n_{l_e}(\mathbf{k}) = \Theta[E_F - E_{l_e}(\mathbf{k})]$, where $\mu = E_F$ is the Fermi energy.

We follow the formalism of Ref. [19] for the model of a quasi-one-dimensional conductor with two dipolar active orbitals per donor and acceptor molecule chain, with tight binding orbital indeces $0_{a(d)}$ and $1_{a(d)}$. The matrix elements of the bare three-dimensional Coulomb electron-electron interaction after the multiple expansion in the long wavelength limit lead to monopole-monopole, monopole-dipole and dipole-dipole contributions reading $V_{0_e 0_f} = \frac{4\pi e^2}{v_0 q^2}$, $V_{0_e 1_f} = \frac{4\pi i e \mu_f q_\parallel}{v_0 q^2}$ and $V_{1_e 1_f} = \frac{4\pi \mu_e \mu_f}{3}\left(\frac{3q_\parallel^2}{q^2} - 1\right) + U_{1_e 1_f}$, respectively, where $U_{1_e 1_f}$ is the short-range part of the Coulomb repulsion, and $\boldsymbol{\mu}_{a(d)}$ is the dipole matrix element oriented along the chain direction $\mathbf{b}$. The volume of the unit cell is $v_0 = abc$, where b is the lattice constant along the chain direction, and a and c are the lattice constants perpendicular to the chain direction.

The microscopic dielectric function equal to the determinant of the system (1) and calculated in Ref. [20] for the present model

$$\varepsilon_m(\mathbf{q},\omega) = \frac{(\omega^2 - \omega_+^2(\mathbf{q}))(\omega^2 - \omega_-^2(\mathbf{q})) - \frac{4\pi e^2}{v_0 q^2}(\Pi_{0a}(q_\parallel,\omega) + \Pi_{0d}(q_\parallel,\omega))(\omega^2 - \omega_{-t}^2)(\omega^2 - \omega_{+t}^2)}{(\omega^2 - E_a^2)(\omega^2 - E_d^2)}. \quad (4)$$

enters into the denominators of all the screened Coulomb matrix elements.

Here

$$\omega_\pm^2(\mathbf{q}) = \frac{1}{2}\left[\omega_a^2(\mathbf{q}) + \omega_d^2(\mathbf{q}) \pm \sqrt{(\omega_a^2(\mathbf{q}) - \omega_d^2(\mathbf{q}))^2 + 16 n_a n_d E_a E_d V_{1_a 1_d}^2(\mathbf{q})}\right] \quad (5)$$

are hybrids of interband dipolar modes from two sublattices $\omega_{a(d)}^2(\mathbf{q}) = E_{a(d)}(E_{a(d)} + 2n_{a(d)}V_{1_{a(d)}1_{a(d)}}(\mathbf{q}))$ with $E_{a(d)}$ being the band separations on corresponding chains and $n_{a(d)}$ being the fractional band fillings. The corresponding transverse hybridised dipolar modes ($\mathbf{q} \perp \mathbf{b}$) are denoted by $\omega_{\pm t}$. Here we take into account that the band separation on both types of chains $E_{a(d)}$, which are of the order of 3 eVs [30] for TTF-TCNQ, are much larger than the corresponding bandwidths with values of the order of 0.5 eVs [31]. The interband electron-hole quasi-continuums reduce, after neglecting bandwidths, to the constant values $E_{a(d)}$ and the sums of the interband polarization diagrams become $\Pi_{01_{a(d)}}(\mathbf{q},\omega) + \Pi_{10_{a(d)}}(\mathbf{q},\omega) = \frac{2n_{a(d)}E_{a(d)}}{\omega^2 - E_{a(d)}^2}$. This approximation is sufficient for considerations at low energies. The intraband RPA polarization diagrams

$$\Pi_{0_{a(d)}}(q_\parallel,\omega) = \frac{4}{N_b}\sum_{k_\parallel = k_F - q_\parallel}^{k_F} \times \frac{E_{0_{a(d)}}(k_\parallel + q_\parallel) - E_{0_{a(d)}}(k_\parallel)}{(\omega + i\eta \mathrm{sign}\omega)^2 - [E_{0_{a(d)}}(k_\parallel + q_\parallel) - E_{0_{a(d)}}(k_\parallel)]^2} \quad (6)$$

are the basic ingredients for the discussion of the dielectric response which follows. Here N_b is the number of the elementary cells along the chains, and k_F is the Fermi wave vector. We consider the tight-binding dispersion of valence bands $E_{0a}(k_\parallel) = -2t_{0a}(\cos k_\parallel b - \cos k_F b)$ and $E_{0d}(k_\parallel) = 2t_{0d}(\cos k_\parallel b - \cos k_F b)$ for acceptor and donor sublattices, respectively. Here $t_{0a(d)}$ are the transfer integrals of valence orbitals along the chains, and energy is measured from the Fermi energy.
The equations

$$E_{0a(d)}(k_\parallel + q_\parallel) - E_{0a(d)}(k_\parallel) = 4t_{0a(d)} \sin\frac{2k_\parallel + q_\parallel}{2} b \sin\frac{q_\parallel b}{2} \tag{7}$$

define the region of the intraband electron-hole quasi-continuums for the wave vectors $k_\parallel$ in the interval $k_F - q_\parallel < k_\parallel < k_F$ and shown as the area in the $(q_\parallel, \omega)$-space in Fig. 1.
The real parts of the polarisation diagrams in Eq. (6) are

$$\Re\mathrm{e}\Pi_{0a(d)}(q_\parallel,\omega) = \frac{2}{\pi}\begin{cases} \dfrac{1}{\sqrt{\omega^2 - \Delta^2_{a(d)}(q_\parallel)}}\left[\arctan v^{>-}_{a(d)} - \arctan v^{>+}_{a(d)}\right], & \omega > \Delta_{a(d)}(q_\parallel), \\ \dfrac{1}{2\sqrt{\Delta^2_{a(d)}(q_\parallel) - \omega^2}}\left[\ln\left|\dfrac{v^{<-}_{a(d)} - 1}{v^{<-}_{a(d)} + 1}\right| - \ln\left|\dfrac{v^{<+}_{a(d)} - 1}{v^{<+}_{a(d)} + 1}\right|\right], & \omega < \Delta_{a(d)}(q_\parallel), \end{cases} \tag{8}$$

where $\Delta_{a(d)}(q_\parallel) = 4t_{0a(d)} \sin\frac{q_\parallel b}{2}$ is the higher edge of the acceptor (donor) electron-hole quasi-continuum and the notations $v^{<\pm}_{a(d)} = \cos\frac{2k_F \pm q_\parallel}{2} b \Big/ \sqrt{1 - \omega^2/\Delta^2_{a(d)}(q_\parallel)}$ and $v^{>\pm}_{a(d)} = \cos\frac{2k_F \pm q_\parallel}{2} b \Big/ \sqrt{\omega^2/\Delta^2_{a(d)}(q_\parallel) - 1}$ are introduced. $\Re\mathrm{e}\Pi_{0a(d)}(q_\parallel, \omega)$ diverges logarithmically at the lower edge of the acceptor (donor) electron-hole quasi-continuum $\delta_{a(d)}(q_\parallel) = 4t_{0a(d)} |\sin\frac{2k_F - q_\parallel}{2} b| \sin\frac{q_\parallel}{2} b$ and at $\delta_{a(d)}(q_\parallel) \leq \Lambda_{a(d)}(q_\parallel) = 4t_{0a(d)} |\sin\frac{2k_F + q_\parallel}{2} b| \sin\frac{q_\parallel}{2} b \leq \Delta_{a(d)}(q_\parallel)$.
The imaginary parts of the intraband polarization diagrams, (6) derived analytically,

$$\Im\mathrm{m}\Pi_{0a(d)}(q_\parallel,\omega) = -\frac{2}{\sqrt{\Delta^2_{a(d)}(q_\parallel) - \omega^2}} \times$$

$$\times\, \Theta(\Delta_{a(d)}(q_\parallel) - \omega)\Theta(\omega - \delta_{a(d)}(q_\parallel)), \tag{9}$$

are different from zero in the region of the electron-hole excitations shown in Fig. 1.
Concerning only the wave vector dependence of the real part of the polarization diagrams, there can be found a peculiarity related to the dimensionality of the system. We note that in the static limit $\Re\mathrm{e}\Pi_{0a(d)}(q_\parallel, 0)$ contains the divergence at $2k_F$ representing the instability of a one-dimensional metal

$$\Re\mathrm{e}\Pi_{0a(d)}(q_\parallel,0) = \frac{1}{|\Delta_{a(d)}(q_\parallel)|\pi} \times$$

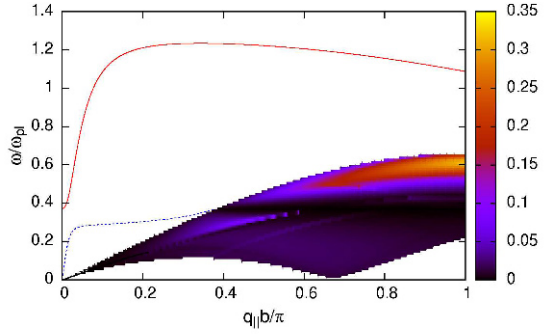

Figure 1. Dispersions of modes $\Omega_1(\mathbf{q})/\omega_{pl}$ (dashed line), $\Omega_2(\mathbf{q})/\omega_{pl}$ (solid line) and $\Omega_4(\mathbf{q})/\omega_{pl}$ between the intraband electron-hole quasi-continuum of TTF and TCNQ bands for $\omega_{pl} = 0.9$ eV, $q_\perp = 0.2\pi/a$ [20] together with the contour plot of the energy-loss function $-\Im\mathrm{m}[1/\varepsilon_M(\mathbf{q},\omega)]/\omega_{pl}$ in the $(q_\parallel, \omega)$-plane and in the range of corresponding quasi-continuums that will be discussed in Section 4.

$$\times\left[\ln\left|\frac{\cos\frac{2k_F - q_\parallel}{2} b - 1}{\cos\frac{2k_F - q_\parallel}{2} b + 1}\right| - \ln\left|\frac{\cos\frac{2k_F + q_\parallel}{2} b - 1}{\cos\frac{2k_F + q_\parallel}{2} b + 1}\right|\right]. \tag{10}$$

Also, we note that $\Re\mathrm{e}\Pi_{0a(d)}(q_\parallel, 0)$ contains a divergence at $4k_F$ when $k_F = \pi/(3b)$, which is the case for TTF-TCNQ. These divergences are the consequence of the planar Fermi surface for one-dimensional bands.

The zeroes of the real part of the microscopic dielectric function (4) determine the energies of the collective excitations in the region outside of an intraband electron-hole quasi-continuum of a quasi-one-dimensional conductor with two kinds of chains. Previously [20], we used the hybrids of interband dipolar modes (5) and the real parts of polarization diagrams (8) in expression (4) to solve the equation $\Re\mathrm{e}\varepsilon_m(\mathbf{q},\omega)=0$, which defines a collective mode dispersion relation of the form $\omega=\Omega(\mathbf{q})$. The real part of the microscopic dielectric function has four zeroes defining the collective modes for the present model, a representative of TTF-TCNQ, calculated in Ref. [20]. It has been shown that the lowest among them, Ω_4, is acoustic for all the directions of the wave vector $\mathbf{q}$ and it appears as a collective excitation due to the opening of a gap in the electron-hole quasi-continuum between the lower edge of the acceptor (donor) contribution $\delta_{a(d)}(q_\parallel)$ and the higher edge of donor (acceptor) contribution $\Delta_{d(a)}(q_\parallel)$ in the long wavelength limit for the longitudinal wave vectors $q_\parallel$. The prediction of such a mode is intrinsic to the quasi-one-dimensional case. Furthermore, mode Ω_1 from Ref. [20] is situated close above both electron-hole quasi-continuums in the long wavelength limit (Fig. 1) and it has a structure that resembles the plasmon modes for a single conducting band of quasi-one-dimensional conductor [13]. Namely, it contains acoustic dispersion in addition to the usual optical branch along the chains. Mode Ω_2 is optic and situated above both electron-hole quasi-continuums for all the directions of the wave vector (Fig. 1) [20]. Mode Ω_1 is assigned to the low frequency excitation at ~10 meV and mode Ω_2 corresponds to the excitation at ~0.75 eV in the infrared optical data of TTF-TCNQ [12, 16–18]. The highest mode, Ω_3, is positioned at a few eVs and is not relevant for considerations of low energies.

From equation (1) we find the screened monopole-monopole Coulomb electron-electron interaction for the present model

$$\overline{V}_{0_a0_a}(\mathbf{q},\omega)=\frac{(\omega^2-\omega_{-t}^2)(\omega^2-\omega_{+t}^2)}{\varepsilon_m(\mathbf{q},\omega)(\omega^2-E_a^2)(\omega^2-E_d^2)}V_{0_a0_a}(\mathbf{q}). \quad (11)$$

After inserting the dielectric function (4) we obtain

$$\bar{V}_{0_a0_a}(\mathbf{q},\omega)=\frac{(\omega^2-\omega_{-t}^2)(\omega^2-\omega_{+t}^2)}{(\omega^2-\omega_+^2(\mathbf{q}))(\omega^2-\omega_-^2(\mathbf{q}))-\frac{4\pi e^2}{v_0q^2}(\Pi_{0a}(q_\parallel,\omega)+\Pi_{0d}(q_\parallel,\omega))(\omega^2-\omega_{-t}^2)(\omega^2-\omega_{+t}^2)}V_{0_a0_a}(\mathbf{q}). \quad (12)$$

We note the strong ω-dependence of the screened Coulomb electron-electron interaction (12). This expresses the dynamic behavior of the screened Coulomb interaction and the necessity of its consideration.

In particular, we consider the case of the orthorhombic counterpart of the TTF-TCNQ lattice with parameters of $t_{0a}=0.15$ eV, $t_{0d}=0.1$ eV, $k_F=0.132a_0^{-1}$ and $U_{1_a1_d}=1.52$ eV. The energy dependence of the real part of the screened Coulomb interaction (12) is determined numerically after taking into account expressions (5) for the hybrids of interband dipolar modes and (8) for the real parts of intraband polarization diagrams. To give the general idea, the result for $q_\perp\neq 0$ is depicted in Fig. 2. The real part of the screened Coulomb electron-electron interaction falls to zero at the lower edge of the electron-hole quasi-continuums and at $\omega=\Lambda_{a(d)}(q_\parallel)$ where $\Re\mathrm{e}\Pi_{0_{a(d)}}(q_\parallel,\omega)$ diverges (Fig. 2 a)), and at the frequency of the lower transverse hybridised dipolar mode $\omega=\omega_{-t}$ (Fig. 2 b)). Also, it diveres at the zeroes of the real part of the microscopic dielectric function $\varepsilon_m(\mathbf{q},\omega)$. In particular, the second divergence in Fig. 2 a) and the divergences in Fig. 2 b) are due to the acoustic collective mode Ω_4 and collective modes Ω_1 and Ω_2, respectively, in the region outside the electron-hole quasi-continuums. The real part of the microscopic dielectric function $\varepsilon_m(\mathbf{q},\omega)$ also contains zeroes in the region of the donor and acceptor electron-hole quasi-continuums resulting in the first and the third divergences in Fig. 2 a).

Next, Fig. 3 represents the plot of the real part of the screened monopole-monopole Coulomb electron-electron interaction versus the longitudinal wave vector in the static limit calculated numerically from expression (12) after taking into account the corresponding intraband polarization diagrams (10) and the longitudinal hybridized dipolar modes $\omega_{\pm l}$ obtained from expression (5) by taking $\mathbf{q}\parallel\mathbf{b}$. We observe from the figure that it falls to zero at the $2k_F$ and $4k_F$ divergences of $\Re\mathrm{e}\Pi_{0_{a(d)}}(q_\parallel,0)$, and it aquires a constant value for $q_\parallel\to 0$. Let us note that, as is seen fom expressions (10) and (12), $\Re\mathrm{e}\Pi_{0_{a(d)}}(q_\parallel,0)=0$ for $q_\parallel\to 0$ leads to a constant value of the real part of the screened Coulomb interaction dependent only on the transverse $\omega_{\pm t}$ and longitudinal $\omega_{\pm l}$ hybridised dipolar

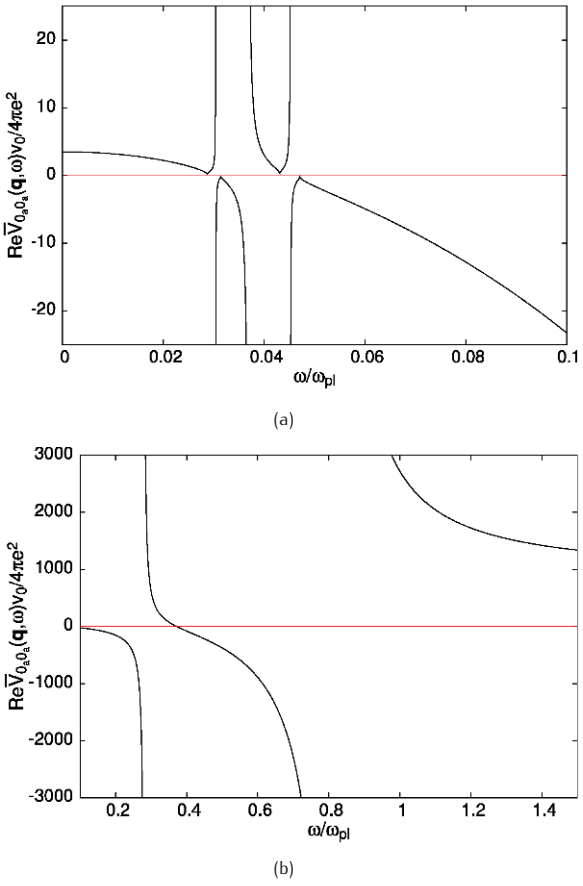

Figure 2. Real part of dynamically screened Coulomb interaction (12) for $q_\perp = 0.2\pi/a$ with $q_\parallel = 0.05\pi/b$.

modes,

$$\Re\mathrm{e}\bar{V}_{0_a0_a}(q_\parallel \to 0, 0) = \frac{\omega_{-t}^2\omega_{+t}^2}{\omega_{-l}^2\omega_{+l}^2}, \tag{13}$$

while $\Re\mathrm{e}\bar{V}_{0_a0_a}(q_\parallel, 0) \to 0$ for $q_\parallel \to \infty$. In the same figure we show, for comparison, the bare Coulomb electron-electron interaction $V_{0_a0_a}(q_\parallel)$.

3. Macroscopic dielectric function

The matrix element ratio of the bare Coulomb interaction to the matrix element of the screened Coulomb interaction defines the macroscopic dielectric function [32] under the condition that the electrons do not change bands, i.e.

$$\varepsilon_M(\mathbf{q}, \omega) = \frac{V_{p_e p_f}(\mathbf{q})}{\bar{V}_{p_e p_f}(\mathbf{q}, \omega)}, \; p_e = (l_e, l_e), \; p_f = (l_f, l_f). \tag{14}$$

The result (12) for the screened Coulomb interaction leads to the macroscopic dielectric function

$$\varepsilon_M(\mathbf{q}, \omega) = \frac{(\omega^2 - \omega_+^2(\mathbf{q}))(\omega^2 - \omega_-^2(\mathbf{q})) - \frac{4\pi e^2}{v_0 q^2}(\Pi_{0a}(q_\parallel, \omega) + \Pi_{0d}(q_\parallel, \omega))(\omega^2 - \omega_{-t}^2)(\omega^2 - \omega_{+t}^2)}{(\omega^2 - \omega_{-t}^2)(\omega^2 - \omega_{+t}^2)}. \tag{15}$$

The ω-dependence of the real and imaginary parts of the macroscopic dielectric function (15), obtained numerically after taking into account the hybrids of interband dipolar modes (5) and the expressions (8) and (9) for the real and imaginary parts of intraband polarization diagrams, are shown in Fig. 4 in the long wavelength limit. The real part of the macroscopic dielectric function diverges at the lower edges of the electron-hole continuums and at $\omega = \Lambda_{a(d)}(q_\parallel)$ (Fig. 4 a)), as well as at $\omega = \omega_{-t}$ (Fig. 4 b)). It has the same zeroes as the real part of the microscopic dielectric function (4). Furthermore, it shows increasing behaviour, passing through the zero Ω_4 between acceptor and donor quasi-continuums (Fig. 4 a)), and the zeroes Ω_1 and Ω_2 (Fig. 4 b)), respectively, while it decreases when passing through the zeroes located in the regions of acceptor and donor quasi-continuums (Fig. 4 a)). The imaginary part of the macroscopic dielectric function (15) is different from zero in the range of the intraband electron-hole quasi-continuum as there $\Im\mathrm{m}\Pi_{0_{a(d)}}(q_\parallel, \omega) \neq 0$. Also, as shown in Fig. 4, it increases in steps at the lower edge of acceptor and donor quasi-continuums as there $\Im\mathrm{m}\Pi_{0_{a(d)}}(q_\parallel, \omega)$, given by expression (9), aquires finite values and diverges at their higher edges, as there $\Im\mathrm{m}\Pi_{0_{a(d)}}(q_\parallel, \omega)$ diverges.

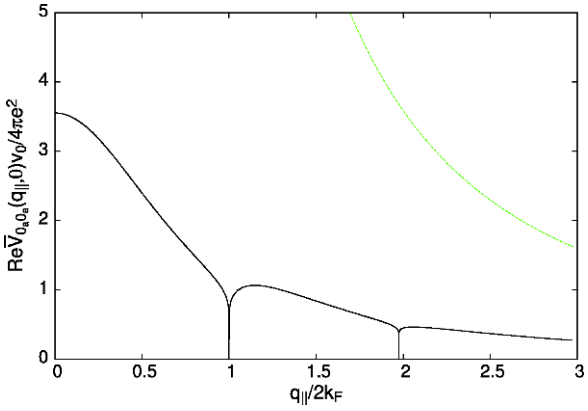

Figure 3. Real part of screened Coulomb interaction (12) for $\omega = 0$ (full line) with the corresponding bare interaction (dashed line).

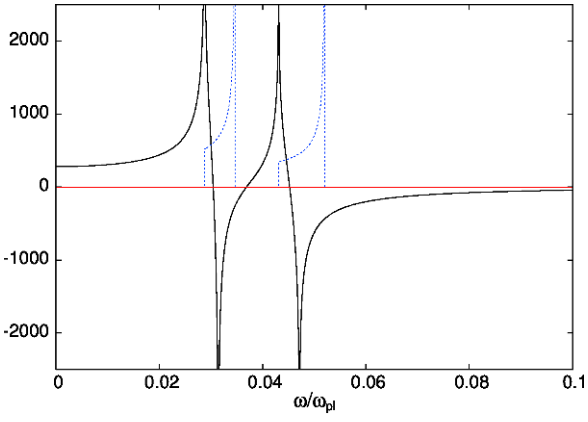

(a)

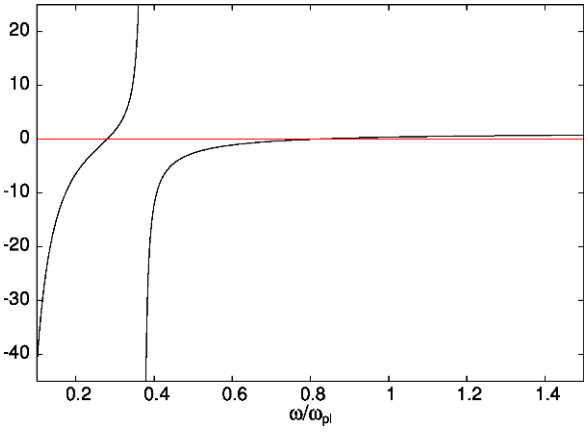

(b)

Figure 4. Frequency dependence of $\Re\mathrm{e}\varepsilon_M(\mathbf{q},\omega)$ (solid line) and $\Im\mathrm{m}\varepsilon_M(\mathbf{q},\omega)/10$ (dashed line) for macroscopic dielectric function (15) with $q_\perp = 0.2\pi/a$ and $q_\| = 0.05\pi/b$.

4. Energy-loss function

The intensity distribution of an EELS spectrum is proportional to the negative imaginary part of the reciprocal value of the macroscopic dielectric function, the energy-loss function [5–7]. Within the present RPA approach this function is nonzero in the region of the electron-hole quasi-continuums and reads

$$
\begin{aligned}
-\Im\mathrm{m}\left[\frac{1}{\varepsilon_M(\mathbf{q},\omega)}\right] &= -\frac{4\pi e^2}{v_0 q^2}(\omega^2-\omega_{-t}^2)^2(\omega^2-\omega_{+t}^2)^2\times \\
&\times(\Im\mathrm{m}\Pi_{0a}(q_\|,\omega)+\Im\mathrm{m}\Pi_{0d}(q_\|,\omega))\times \\
&\left\{\left[(\omega^2-\omega_+^2(\mathbf{q}))(\omega^2-\omega_-^2(\mathbf{q}))-\frac{4\pi e^2}{v_0 q^2}(\Re\mathrm{e}\Pi_{0a}(q_\|,\omega)+\right.\right. \\
&\left.+\Re\mathrm{e}\Pi_{0d}(q_\|,\omega))(\omega^2-\omega_{-t}^2)(\omega^2-\omega_{+t}^2)\right]^2 \\
&+\left[\frac{4\pi e^2}{v_0 q^2}(\Im\mathrm{m}\Pi_{0a}(q_\|,\omega)+\Im\mathrm{m}\Pi_{0d}(q_\|,\omega))\times\right. \\
&\left.\left.\times(\omega^2-\omega_{-t}^2)(\omega^2-\omega_{+t}^2)\right]^2\right\}^{-1}, \qquad (16)
\end{aligned}
$$

as follows from expression (15). Outside of this region it acquires a value of zero except at zero $\Omega(\mathbf{q})$ of the real part of microscopic dielectric function (4) where it is represented by the δ-peak

$$
-\Im\mathrm{m}[1/\varepsilon_M(\mathbf{q},\omega)] = Z(\mathbf{q})\pi\delta(\omega-\Omega(\mathbf{q})) \qquad (17)
$$

with

$$Z(\mathbf{q}) = \frac{(\Omega^2(\mathbf{q}) - \omega_{-t}^2)(\Omega^2(\mathbf{q}) - \omega_{+t}^2)}{\frac{\partial}{\partial\omega}\left[\omega^2 - \omega_+^2(\mathbf{q}))(\omega^2 - \omega_-^2(\mathbf{q})) - \frac{4\pi e^2}{v_0 q^2}(\Re\mathrm{e}\Pi_{0a}(q_\parallel,\omega) + \Re\mathrm{e}\Pi_{0d}(q_\parallel,\omega))(\omega^2 - \omega_{-t}^2)(\omega^2 - \omega_{+t}^2)\right]\Big|_{\Omega(\mathbf{q})}}. \quad (18)$$

Thus, the energy-loss function gives the strength of the various excitations. The numerical results for the electron energy-loss function, obtained after taking into account expressions (5), (8) and (9) for $\omega_\pm$, the real and imaginary parts of $\Pi_{01a(d)}(q_\parallel,\omega)$ as well as the zeroes $\Omega_{1,2,4}(\mathbf{q})$ of the real part of the dielectric function (4), are presented in Figs. 1 and 5. In particular, Fig. 1 shows the contour plot of the electron energy-loss function in the $(q_\parallel,\omega)$-plane and in the region of the intraband electron-hole quasi-continuum together with the lines which indicate the dispersions corresponding to the collective modes, while Fig. 5 shows the contour plot of the entire electron energy-loss function. As it is seen in Figs. 1 and 5 the electron energy-loss function comprises two sharp peaks belonging to modes Ω_1 and Ω_2, while the intraband electron-hole quasi-continuum shows up as a continuous contribution. The energy-loss function reveals that in the long-wavelength limit the intraband electron-hole quasi-continuum and low-energy acoustic mode Ω_4 have negligible spectral weight. Thus they may be experimentally unobservable. Also, the spectral weight of acoustic collective mode Ω_1 slightly dominates over the spectral weight of optical mode Ω_2, and both should be detectable. Furthermore, for the intermediate longitudinal wave vectors $q_\parallel$ (Figs. 1 and 5) mode Ω_1 transfers all of its weight to the weak broad structure in the energy-loss function as it approaches the boundary of the intraband electron-hole quasi-continuum and to mode Ω_2 which now carries most of the spectral weight. However, for large longitudinal wave vectors $q_\parallel$ mode Ω_2 loses some of its weight in favour of the intraband electron-hole quasi-continuum as it shifts to lower energies. Simultaneously, the energy-loss function obtains a well defined broad structure with significant spectral weight, observable in experiments, in the upper part of the intraband electron-hole quasi-continuum. This structure appears because the zero Ω_1 of the real part of the macroscopic dielectric function enters into the region of the intraband electron-hole quasi-continuum. The results obtained are in accordance with the data of Ritsko et al. [12] who have reported a decrease in the strength of the 0.75 eV collective mode as the first Brillouin zone edge is approached. They suggest that this decrease may be due to increasing intraband electron-hole quasi-continuum spectral weight.

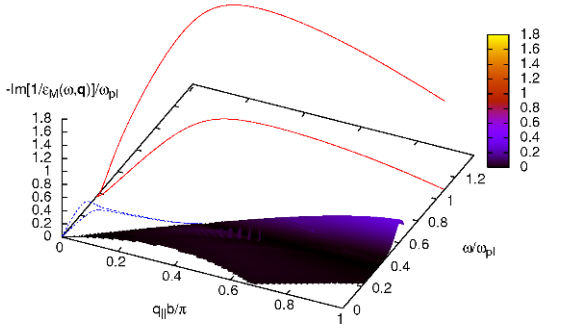

Figure 5. Energy-loss functions $-\Im\mathrm{m}\left[1/\varepsilon_M(\mathbf{q},\omega)\right]/\omega_{pl}$ for $q_\perp = 0.2\pi/a$. Lines indicate the strength $Z(\mathbf{q})\pi/\omega_{pl}$ of δ-peaks in the energy-loss function that belong to collective mode dispersions $\Omega_1(\mathbf{q})$ (dashed line) and $\Omega_2(\mathbf{q})$ (solid line).

5. Conclusion

In conclusion, we have studied the dynamical screening properties for the model of a quasi-one-dimensional conductor with four orbitals per primitive cell. The present analysis shows that hybridized collective modes and the intraband electron-hole quasi-continuum regulate the RPA screened monopole-monopole Coulomb electron-electron interaction, the macroscopic dielectric function and the structure of the electron energy-loss function. Also, the present analysis indicates the importance of the long-range dipole Coulomb electron-electron interaction for dielectric screening and the energy-loss properties of TTF-TCNQ as strong dipole Coulomb interactions leading to strong coupling between intraband plasmon and interband dipolar modes result in hybridized collective modes. Regarding the electron energy-loss function, full dependence on the wave vector and frequencies has been explored. It comprises the contributions from collective modes and from the intraband electron-hole quasi-continuum. We find that the two modes placed just above the electron-hole quasi-continuum, the renormalised acoustic plasmon and the dipolar mode, carry most of the spectral weight in the long wavelength limit for TTF-TCNQ. For large longitudinal wave vectors we find an interesting and unexpected broad feature in the energy-loss function in the region of intraband

electron-hole quasi-continuum which follows the zero of the real part of the macroscopic dielectric function corresponding to the renormalized plasmon collective mode, together with the contribution from the δ-peak belonging to the optical dipolar mode. The results obtained are in accordance with the early experimental EELS data of TTF-TCNQ which showed a loss of dipolar mode spectral weight in the range of large longitudinal wave vectors along with negative dispersion [12]. Thus, the present analysis also indicates the importance of intraband excitations in the interpretation of the EELS data of TTF-TCNQ for large wave vectors.

Finally, the present work is for zero temperature, as it is pointed in the Introduction. Let us note that our preliminary considerations of the extension to finite temperatures show that dispersions of collective modes for temperatures above 60 K behave qualitatively the same as the ones obtained in $T = 0$ formalism[1]. Moreover, in this way one can follow continously how these dispersions and the energy-loss function vary as one passes from room temperature to the temperature of charge density wave transition. This question is under current investigation.

References

[1] Y. Takahashi et al., Appl. Phys. Lett. 88, 073504 (2006)
[2] K. Shibata et al., Appl. Phys. Lett. 90, 193509 (2007)
[3] M. Sakai et al., Synthetic. Met. 153, 293 (2005)
[4] T. Hagesawa, J. Takeya, Sci. Technol. Adv. Mat. 10, 024314 (2009)
[5] D. Pines, Elementary excitations in solids (McGraw-Hill Book Company, New York, 1971)
[6] J. Fink et al., J. Electron Spectrosc. 117, 287-309 (2001)
[7] R. F. Egerton, Rep. Prog. Phys. 72, 016502 (2009)
[8] L. Hedin, S. Lundqvist, In: F. Seitz, D. Turnbull (Ed.), Solid state physics 23 (New York, Academic, New York, 1969) 1
[9] S. Hüfner et al., J. Electron Spectrosc. 100, 191 (1999)
[10] S. Hüfner, Springer Series Soli. 82, 1 (2003)
[11] A. Bostwick et al., Science 328, 999 (2010)
[12] J. J. Ritsko et al., Phys. Rev. Lett. 34, 1330 (1975)
[13] P. F. Williams, A. N. Bloch, Phys. Rev. B 10, 1097 (1974)
[14] P. F. Williams, A. N. Bloch, Phys. Rev. Lett. 36, 64 (1976)
[15] L. M. Khan, J. Ruvalds, Phys. Rev. B 17, 4600 (1978)
[16] D. B. Tanner et al., Phys. Rev. B 13, 3381 (1976)
[17] C. S. Jacobsen, Lect. Notes. Phys. 95, 223 (1979)
[18] H. Basista et al., Phys. Rev. B 42, 4088 (1990)
[19] P. Županović, A. Bjeliš, S. Barišić, EPL-Europhys. Lett. 45, 188 (1999)
[20] Ž. Bonačić Lošić, P. Županović, Cent. Eur. J. Phys. 8, 283 (2010)
[21] S. Das Sarma, A. Madhubar, Phys. Rev. 23, 805 (1981)
[22] S. Das Sarma, E. H. Hwang, Phys. Rev. B 54, 1936 (1996)
[23] S. Das Sarma, E. H. Hwang, Phys. Rev. B 59, 10730 (1999)
[24] B. Wunsch et al., New J. Phys. 8, 318 (2006)
[25] E. H. Hwang, S. Das Sarma, Phys. Rev. B 75, 205418 (2007)
[26] M. Polini et al., Phys. Rev. B 77, 081411 (2008)
[27] P. K. Pyatkovskiy, J. Phys.-Condens. Mat. 21, 025506 (2009)
[28] E. H. Hwang, S. Das Sarma, Phys. Rev. B 80, 205405 (2009)
[29] A. L. Fetter, J. D. Walecka, Quantum theory of many-particle systems (W. A. Benjamin, Inc., New York, Amsterdam, 1964)
[30] A. S. Pennelly, C. J. Echardt, Chem. Phys. 12, 89 (1976)
[31] D. Jérome, H. J. Schulz, Adv. Phys. 31, 299 (1982)
[32] P. Županović, A. Bjeliš, S. Barišić, Z. Phys. B Con. Mat. 101, 387 (1996)